# Analysis of seafloor marine EM data with respect to motion-induced noise

**K. M. Bhatt[1], A. Hördt[1] and T. Hanstein[2]**

[1]Inst. f. Geophysik u. Extraterrestrische Physik, TU Braunschweig

[2]KMS Technologies - KJT Enterprises Inc.

## Abstract

Any appreciable movement of sea water induces an electromagnetic field, which acts as noise for marine controlled source electromagnetic (mCSEM) data. Noise in seafloor mCSEM data is considered small, but since the characteristic reservoir signal is also small, the understanding and possible removal of noise may be essential to increase the number of possible target reservoirs.

A power spectral density plot of the time-series extracts the power of each frequency contribution, but the shortcoming is that the time information is lost. To get time information corresponding to each frequency, we plotted a spectrogram which shows how the spectral density of a signal varies with time. The collective use of these three plots, i.e. time series, power spectral density and spectrogram, helps to analyse the information concealed in the time-series. In a measured signal-free mCSEM data, we are able to identify various oceanic features like microseisms, swell etc, which play a significant role in inducing an electric field.

**Key words**: mCSEM, Swell, Microseisms

---

## 1. Introduction

Marine controlled source electromagnetic (mCSEM) data is generally contaminated by some unwanted electromagnetic (EM) signals ambient at the seafloor. Understanding and possible removal of the noise is essential as technology is advancing from deep ocean to shallow ocean, where the noise is much more effective.

In general, there could be two possible sources of oceanic noise production. Internal oceanic processes or any other external influences like ionospheric and magnetospheric current systems. Faraday (1832) reported that any appreciable movement of seafloor and sea water by induction generates electromagnetic signals with in the ocean. Motional induction got more attention after world war II, with the detailed oceanic induction study by many authors like Sanford (1971), Podney (1975), Chave and Cox (1982), Chave and Luther (1990). Similarity in all these studies is that they all

studied the theoretical aspect of motional induction occurring due to various movements in the ocean. Experimental evidence was provided by Webb and Cox (1986), who made a nice comprehensive study about the seafloor microseisms by observing pressure and electric field spectra at the seafloor.

Wave progressions and oceanic processes are, usually, a function of the regional and local conditions. A variety of motional processes like swell, ripples, internal waves, microseisms, hum etc generate a range of EM noise at the seafloor, which varies from place to place. External, ionospheric and magnetospheric, current systems also contribute EM noise, but they are limited to the lower frequency range due to the conductive filtering of the ocean. Characteristics of the noise are poorly known till now, as only few studies are made. The present study is dedicated to the understanding of the noise characteristics at the sea floor.

For the study, a marine EM data set recorded at the seafloor in the absence of a transmitter, is used. Recording is made for two horizontal components of electric fields i.e. $E_x$ and $E_y$, which are perpendicular to each other. Visibly, $E_x$ and $E_y$ time series data appears different in their pattern and amplitudes despite the same oceanic environment. This suggests that a comprehensive study on the directional characteristics of the events/sources of noise could play a decisive role in identifying the noise sources.

The oscillatory occurrence, due to a disturbance, can be comfortably visualised in frequency domain. The power spectral density (PSD) of each frequency contribution helps in marking the power of the individual sources. But the shortcoming of the PSD calculation is that if the source of the characteristic frequency is not known a priori, it is difficult to conclude about the source environment with the frequency information only. In this case, time information together with the PSD may help at least to distinguish between localised and ambient sources, which itself is of significant use. To overcome the PSD shortcoming to retain time information corresponding to each frequency, spectrograms are plotted, which show how the spectral density of a signal varies with time.

In the signal-free mCSEM data, we have observed many features which are new for mCSEM studies. The spectrogram presents clear prints of oceanic features like microseisms and swell, which play a significant role in inducing an electric field at the seafloor.

## 2. Marine Controlled Source Electromagnetism (mCSEM)

A mCSEM data acquisition methodology is shown in Figure 1. In practice, an EM transmitter is towed close to the seafloor to maximize the coupling of electric and

magnetic fields with seafloor rocks. These fields are recorded by instruments deployed on the seafloor at some distance from the transmitter. Details about the data acquisition practice in both time and frequency domain of mCSEM is well documented in the article by Constable and Srnka, (2007).

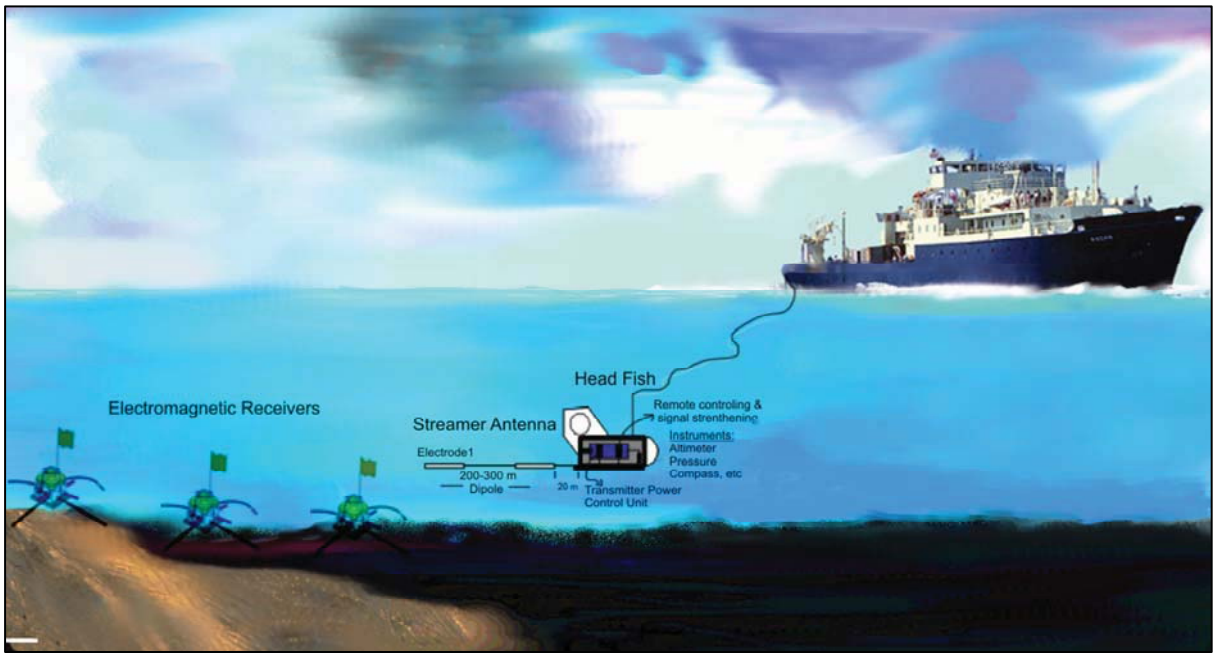


**Figure 1: Schematic diagram showing field layout for mCSEM sounding.**

## 3. Sources of mCSEM noise

The noise convolved in mCSEM data is capable of masking significant marine information. Broadly, two origins are expected as noise sources in mCSEM data:-

a) **External origin:** The magnetospheric and ionospheric current system induces natural electric and magnetic (EM) fields in the conductive formations. The induced fields are signal for the magnetotelluric (MT) technique but noise for mCSEM data. The conductive ocean filters the higher frequencies. The skin depth ($\delta$) is given by

$$\delta \approx 503\sqrt{\frac{1}{\sigma f}}$$

This implies, $f \approx 76{,}000 / \delta^2$ for $\sigma = 3.3$ S/m

Therefore, at the ocean floor the external origin fields effectively contribute frequencies less than or equal to $f = (76{,}000/ D^2)$, where D is the depth of ocean floor in meters and f is given in (1/s). As example for an ocean of depth 500 m, the external field will contribute frequencies less than 0.3 Hz at the sea floor. This

suggests that the frequencies higher than 0.3 Hz could be by internal oceanic origin.

b) **Internal origin:** The dynamics of oceanic water with in the ambient geomagnetic field induces electric and magnetic field in the ocean. A frequency range of the fields is generally $0.3 < f\ (Hz) < 16$ (Dahm et. al., 2006) excluding long period waves like tidal waves, tsunami, seiches and storm surge etc.

Other than these noise sources, there are processes like earthquakes, volcanoes, manmade explosions etc occurring at the vibrant ocean floor, which add noise in mCSEM data.

## 4. Motional induction

The ocean is an electrically conducting fluid containing the ionic charge particles. Moving charge particles in the ambient geomagnetic field experience a deflective Lorentz force. If $\vec{v}$ is the velocity of charge particle q moving in the geomagnetic field $\vec{B}$, then the Lorentz force is-

$$\vec{F}_L = q(\vec{v} \times \vec{B}) \qquad (1)$$

The charge q experiences the deflecting force $\vec{F}_L$ because of the action of an electric field which we call Lorentz electric field ($\vec{E}_L$),

$$\vec{F}_L = q\vec{E}_L \qquad (1\text{-a})$$

$$\vec{E}_L = \vec{v} \times \vec{B} \qquad (2)$$

The field $\vec{E}_L$ generates a secondary electric field $\vec{E}$, mainly by two processes: i) Galvanic process, ii) Inductive process (Bhatt et al, 2010). For a stationary frame of reference, the current density in the Ohms law is given by

$$\vec{J} = \sigma(\vec{E} + \vec{E}_L) = \sigma(\vec{E} + \vec{v} \times \vec{B}) \qquad (3)$$

Here, $\sigma$ is the conductivity of the ocean, $\sigma\vec{E}$ is the current term generated by both a galvanic and an inductive process and $\sigma(\vec{v} \times \vec{B})$ is the source current term for the motional induction case. Under the quasi-static approximation, the set of Maxwell's equation to be solved for the motional induction case is

$$\nabla \times \vec{H} = \sigma(\vec{E} + \vec{v} \times \vec{B}_0)$$
$$\nabla \times \vec{E} = -\mu_0 \partial_t \vec{H} \qquad (4\text{-a,b})$$

Simplification of the source $\sigma(\vec{v}\times\vec{B})$ in terms of component $J_x, J_y$ and $J_z$ can be written as,

$$\begin{aligned} J_x &= \sigma(E_x + v_y B_z - v_z B_y) \\ J_y &= \sigma(E_y + v_z B_x - v_x B_z) \\ J_z &= \sigma(E_z + v_x B_y - v_y B_x) \end{aligned} \tag{5}$$

The non-divergent requirement condition of the current (i.e. $\nabla.\vec{J} = 0$) suggests that the current will close its loop with in the earth rather than closing in the ocean. Therefore, the horizontal electric currents (i.e. $J_x$ and $J_y$) in the ocean are more effective than the vertical currents (i.e. $J_z$) as the horizontal extent of ocean is much larger than the vertical depth. In mCSEM, the data is recorded at the seafloor, where normally the vertical velocity component (i.e. $v_z$) is very small. Therefore, terms $v_z B_y$ and $v_z B_x$ is negligible. Above argument simplifies (4),

$$\begin{aligned} J_x &= \sigma(E_x + v_y B_z) \\ J_y &= \sigma(E_x - v_x B_z) \end{aligned} \tag{6}$$

Using (6), simplification of (4-a) gives

$$\begin{aligned} E_x &= -\left(\frac{1}{\sigma}(\partial_z H_y - \partial_y H_z) + v_y B_z\right) \\ E_y &= +\left(\frac{1}{\sigma}(\partial_z H_x - \partial_x H_z) + v_x B_z\right) \end{aligned} \tag{7}$$

Where the first term is the induced field and second term is the source term. Normally, the area used for mCSEM data acquisition is very small to observe horizontal variation in the vertical magnetic field $H_z$. Therefore, term $\partial_y H_z$ and $\partial_x H_z$ are negligible. Finally, we have a simplified equation,

$$\begin{aligned} E_x &= -\left(\frac{1}{\sigma}\partial_z H_y + v_y B_z\right) \\ E_y &= +\left(\frac{1}{\sigma}\partial_z H_x + v_x B_z\right) \end{aligned} \tag{8}$$

Noticeably, the horizontal particle motion (i.e. $v_x$ and $v_y$) is source for the induction of the horizontal electric field (i.e. $E_x$ and $E_y$).

## 5. The Data

We have analysed horizontal component electric field (i.e. $E_x$ and $E_y$) data recorded at 500 m depth on the ocean floor. The recording is made in the absence of transmitter current to understand the oceanic background noise. Time series is shown in Figure 2. It is evident that the strength and pattern of $E_x$ and $E_y$ are different.

In equation (8), the first term is much smaller than the second term (i.e. $(1/\sigma)\partial_z H_{y|x} << v_{y|x} B_z$), suggesting x-and y- component of velocity principally controls the strength of the $E_y$ and $E_x$ component of the electric field respectively. Evidently, the strength of $E_x$ is higher than $E_y$ (Figure 2). This suggests that the wave velocity in the y-direction will be higher than the x-direction (i.e. $v_y > v_x$). Further, as normally the surface wave moves towards the coast. Accordingly, the velocity component pointing towards the coast has higher velocity than the other horizontal component. The present data is recorded with a setting that the y-component of the receiver points towards the cost and constructs an angle of approx. 55° with it. Thus, the data acquisition setting as well favours for $v_y > v_x$. In general, electric field measurements characterize an average motion over the length of the antenna. Therefore electric field components can be used to derive information about the average velocity of the movements.

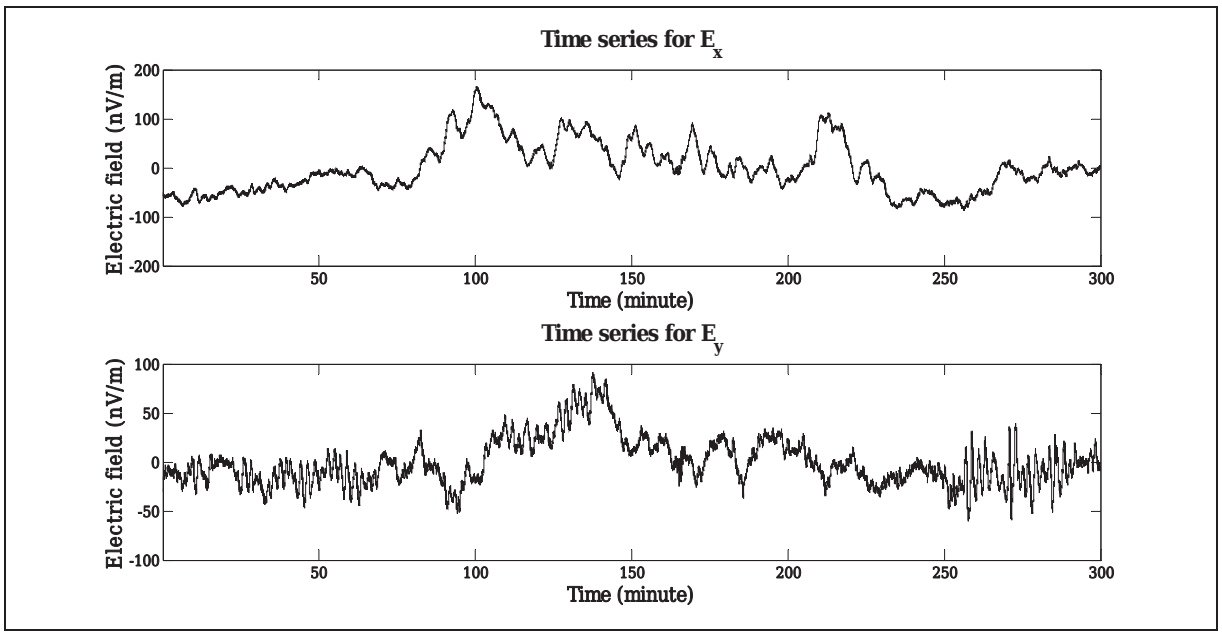


**Figure 2: Five hour times-series of two horizontal components of electric fields.** $E_x$ (top) and $E_y$ (bottom). The recording is made at the seafloor, 500 m below the sea surface.

## 6. Power Spectral Density (PSD) and Spectrogram

Power spectral density is calculated to study the power content of the frequencies. For the PSD calculation, steps followed are as follows:

I. *Inspection of time series (Figure 2):* Inspection is done to recognize glitches or other outliers in the data that are not consistent with the rest of the time series.

II. *Detrending*: Detrending ensures that the first Fourier coefficient does not dominate the PSD.
III. *Windowing:* A Hanning window is applied to minimise the leakage of spectral density.
IV. *Calculation of discrete Fourier transform (DFT):*
V. *Calculation of PSD:* PSD is calculated by segment averaging method (Welch, 1967).

The PSD for Ex and Ey is shown in Figure 3. Over all spectral power is decreasing with increase in frequency. Four different slopes can be seen in the both PSD's (Ex and Ey). Let the slope containing frequencies between 0.001 – 0.1 Hz, 0.1 - 2 Hz, 2 – 10 Hz and 10 - 25 Hz represent respectively low, intermediate, sub-high and high frequency range. Evidently, in the low frequency range the power of the electric field rises sharply. Generally, external origin field mainly affects the low frequency range, as higher frequencies are filtered out by the ocean resulting in passage for low frequencies only (i.e. less than 0.3 Hz for a 500 m deep ocean) to the ocean bottom due to skin depth. The oceanic eddies (very long wavelength oceanic feature) are another low frequency source (Chave and Filloux, 1984). Here, these two sources are presumed for the sharp rise in power in the low frequency range (0.001 – 0.1 Hz). In the range of intermediate frequency, four peaks are evident, at 0.2, 0.3, 0.4 and 1 Hz, in the PSD representing that this frequency range is receptive for the various oceanic flows close to seafloor. The sub-high frequency range is nearly flat. A flat PSD, generally, corresponds to a field which contains equal power within a fixed bandwidth which resembles noise. In the high frequency range a sharp rise is evidenced which is presumed due to digitisation noise.

The frequency and power information of a PSD is insufficient to characterise the source process corresponding to the frequencies. Time preservation may help in this subject. Together with the frequency and power, information about time may help in identifying and characterising the source nature of process. The localised time process may represent a source progressing in an interval of time while an ambient time process reflects a continuous process. For the purpose therefore spectrograms are plotted which preserve the time information together with frequency and power. The spectrogram is the discrete-time Fourier transform for a sequence, computed using a sliding window. For a spectrogram calculation, the time series is divided in to segments equal to the length of the hamming window. Each segment overlaps 50% of the samples with the adjacent segment and then PSD is calculated for a defined frequency length. Again and again PSD is calculated by sliding the window to build a spectrogram. The Spectrograms corresponding to time series shown in Figure 2 is shown in Figure 5. There are three

distinct anomalous features evident in spectrograms. One feature is corresponding to time approx. 165 min (like spike) and other two are at frequencies 1, 0.3 Hz. It is difficult to confidently propose a source nature for the spiky feature at approx. 165 min. This could be due to either by a regional earthquake or by a volcano like feature. In general, regional earthquakes are found in band frequencies of 0.1 to 1 Hz and here the spiky feature correspond the same range. The other two features at frequencies 1 and 0.3 Hz are respectively by the microseisms and swell, that will be discussed in the next section.

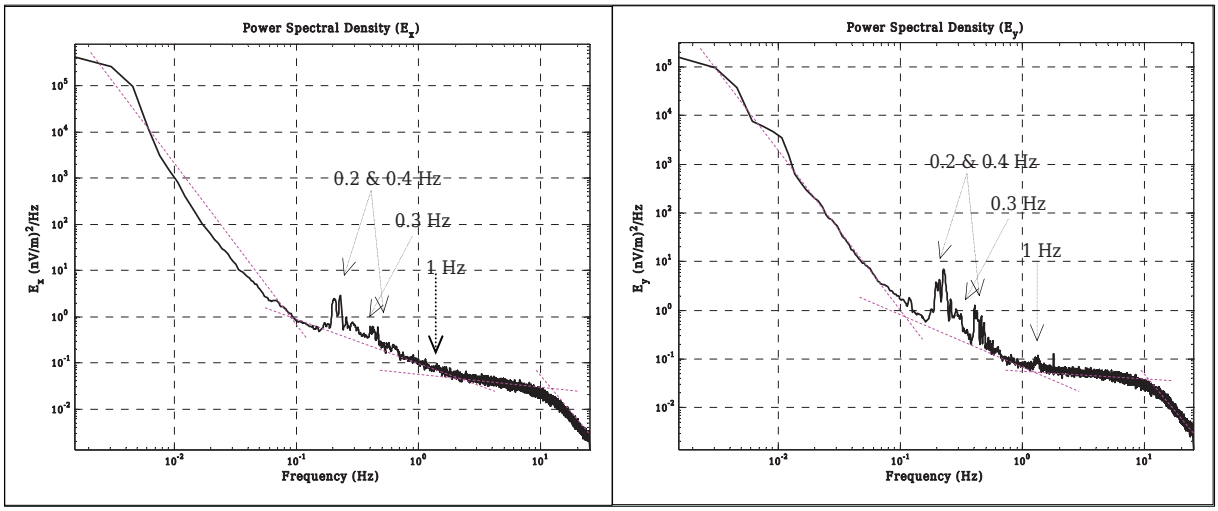


**Figure 3: Spectra of the two horizontal electric components $E_x$ and $E_y$ corresponding to time series shown in Figure 2**. The graphs show the PSD vs. frequency. The anomalous peaks are visible at 0.2, 0.4 and 1 Hz. There is also a weaker peak at 0.3 Hz. Four slopes can be observed in the spectra (pink dashed lines).

## 7. Microseisms and swell

Microseisms are like a soft earth tremor originating with in the ocean by non linear interaction of oceanic waves, which causes a continuing oscillation of the ocean floor. The broad frequency range for microseisms is between 0.05 to 1 Hz, which mainly depends on the ocean depth and oceanic conditions.

Languet-Higgins (1950) proposed a mechanism for microseisms (0.05 -2.0 Hz) and showed that if two identical progressive waves travelling in opposite directions interact with each other, there is a second order pressure term effect which does not vanish with depth and can thus reach the deep ocean bottom (Figure 4). Consider two surface waves of frequencies $f_1$ and $f_2$ ($f_1 \approx f_2$), moving with approx. same velocity in opposite direction. Let the wave number of frequencies are respectively $k_1$ and $-k_2$, and then $k_1 \approx -k_2$. Interaction of these waves will leave behind a wave with very small wave number {i.e. $k_1 + (-k_2)$ = diminutive} and very large wavelength. The large wavelength is capable of creating a pressure disturbance effectively at the ocean floor. The amplitude of the

pressure disturbance is proportional to the product of the interacting wave heights and the frequency. These pressure fluctuations in the water column might then excite Rayleigh waves in the solid earth and be observed as microseisms.
In short, the favourable oceanic conditions for microseisms generation are:

1. Shoreline geological setting creating grounds for nonlinear interaction of surface waves.
2. Near shore reflection of high frequency surface waves and thereafter head on interaction.
3. A fast moving storm creating a sequence of wave in different directions.
4. High frequency wave interaction may generate whitecaps (a wind blown wave whose crest is broken and appears white), which leads in acoustic energy transmission to ocean bottom.

The depth of the ocean is another important factor in microseisms generation. The wave generation in the ocean depends on the wind velocity, which become efficient when the wave velocity is close to the phase velocity of the ocean waves. Velocity of ocean wave (V) is, roughly speaking, $\sqrt{(gD)}$, where D is ocean depth and g is acceleration due to gravity. Therefore, for a 4 km deep ocean and a 500 m shallow ocean, the velocity V is approximately 200 m/s and 70 m/s respectively. A typical wind velocity rarely exceeds few tens of m/s. This suggests wind velocities are quite close to the oceanic velocities especially in the shallow oceans. Therefore the generation of microseisms is likely to be efficient in shallow oceans (Tanimoto, 2005).

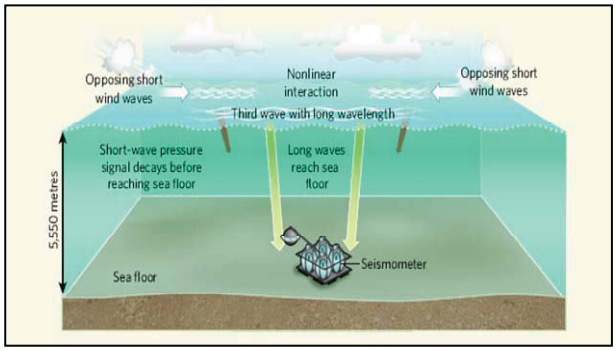


**Figure 4: Microseisms mechanism** (from Elgar (2008)). Nonlinear interaction of short opposing waves leads to a long wavelength wave generation, which reaches the seafloor and generates

Swells are a kind of oceanic surface waves. They are often created by the breaking of storms thousands of kilometres away from the seashore. The distance allows the waves comprising the swells to become more stable, clean, and continuous as they travel toward the coast. For microseisms generation, in general, higher frequency waves are more efficient than the lower frequency waves like swells. Swells are more directional and therefore chances for non linear interaction is not as much as of higher frequency gravity waves (Webb and Cox, 1986), which are generated with in the ocean by the influence of gravity at the interface involving the density contrast. In Figure 3 and 5,

the anomalous feature close to 1 Hz is likely due to a microseism. A microseism is a time localised feature, the duration of which depends on the time of effective nonlinear wave interaction. It is evident from Figure 5 that close to 1 Hz, there are four time localised features ($E_y$ component has more clear appearance than $E_x$), corresponding to time 8, 40, 90 and 250 min approx. Further evidence in support of microseisms is the observed frequency (i.e. 1 Hz).

The acquired electric field data was recorded in a shallow ocean (500 m depth). Normally, a shallow ocean may contribute the microseisms in high frequency range (i.e close to 1 Hz) as analogous to high frequency even a comparable wavelength (not necessary a huge wavelength) may reach ocean bottom to produce microseisms. The mechanism of microseisms generation suggests that maximum electric field power will be experienced in the component perpendicular to the direction of wave propagation. Here, the velocity component $V_y > V_x$ as amplitude of $E_x > E_y$. The strong power of microseisms in the $E_y$ component compared to the $E_x$ component further supports to interpret 1 Hz frequency as microseisms.

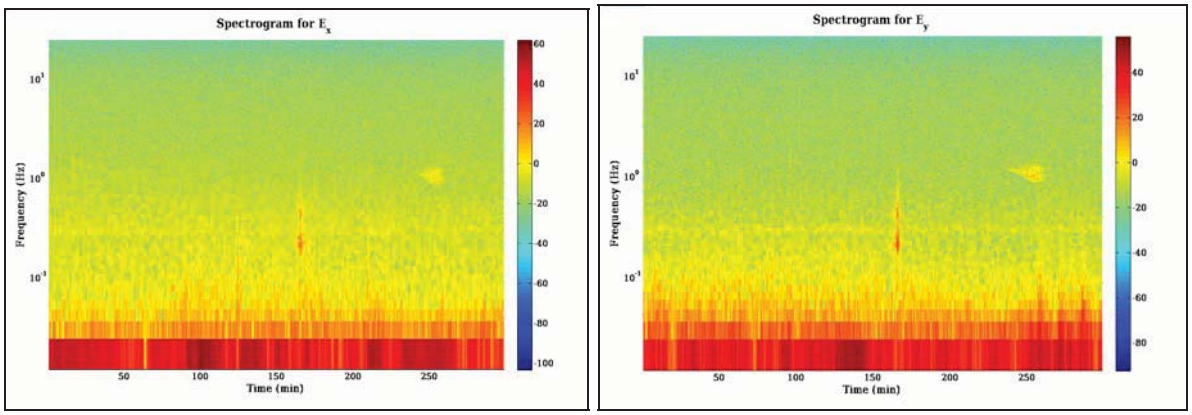


**Figure 5**: **Spectrogram for $E_x$ & $E_y$.** Electric field power is colour coded in dB and displayed as function of time and frequency. Two anomalous features are visible, one at 1 Hz and the other covering a broad frequency range, having max. power at 0.2 & 0.4 Hz.

The individual feature ambient in time at 0.3 Hz (Figure 3 & 5) is interpreted here as a swell. A swell consists of long-wavelength surface waves which are more stable in their directions and frequency than normal wind waves. Swells are dispersive in nature and their frequency is given by $\omega^2 = gs \tanh(sD)$, where g is acceleration of gravity; $s = 2\pi/\lambda$ is wave number, $\lambda$ is the wavelength of the swell and D is the depth of ocean. A calculation suggests that a swell of frequency 0.3 Hz corresponds to a wavelength of 18 m for 500 m deep oceanic water. The obtained wavelength is well in range for the

wavelengths of swells. As 0.3 Hz frequency is evident throughout the time in spectrogram (Figure 5), this is another strong support for 0.3 Hz to stand for a swell.

## 7. Microseisms during mCSEM data recording

Microseisms are a powerful feature to effectively generate EM signal at the ocean floor. They are quite capable of masking the mCSEM signals. We have an example comparing the power of microseism and mCSEM transmitter current. In Figure 5, we have seen the spectrograms of mCSEM the time-series recorded in the absence of transmitter current. On the other hand, Figure 6 represents spectrograms of the mCSEM data when transmitter was transmitting signals. Systematic decay in the power is evident in Figure 6, representing transmitter is moving away from the receiver. A gathering of high power (yellow colour) patch is evident corresponding to frequency 0.1 Hz and time 200 min, may be representing a microseism. Clearly, the power of a microseism is significant enough to contaminate the mCSEM data. It is as well evident that the effect of swell is feeble in the presence of a transmitter current. For a larger transmitter receiver distance this effect may be significant.

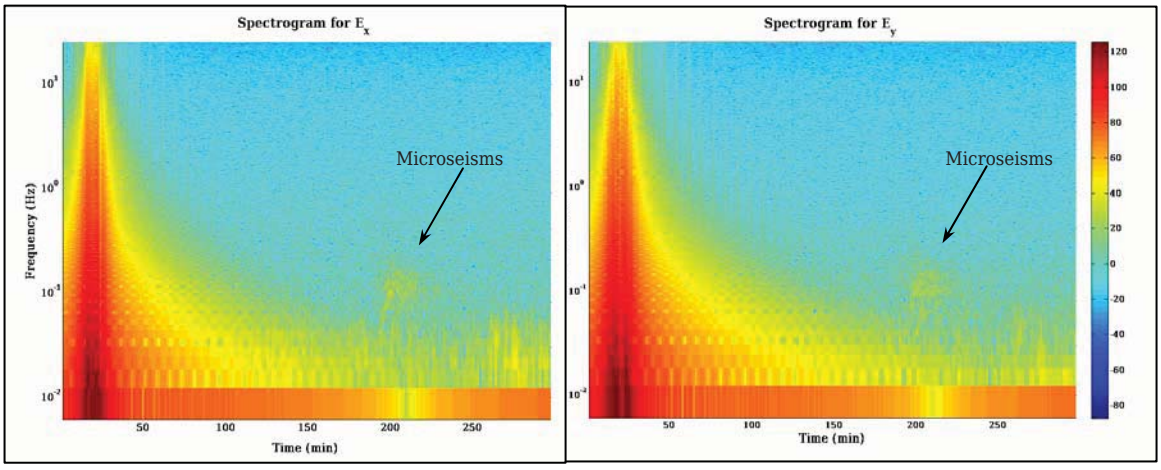


**Figure 6: Presence of a microseism during mCSEM data recording.** Electric field power is colour coded in dB and displayed as function of time and frequency. Corresponding to frequency 0.1 Hz and time 200 min (approx), a yellow coloured high power patch is evident, which may be is by a microseism. The other efficient high power patches in the spectrogram is by the transmitter current

## 8. Conclusions

By the analysis seafloor electric field data, we provide evidence for the observation of microseisms and swell in mCSEM data. Power spectral density (Figure 3) and

spectrogram (Figure 5) clearly present the evidence for the possible presence of microseism and swell corresponding to the frequencies 1 Hz and 0.3 Hz respectively. Swells are time ambient oceanic feature, which can be clearly marked in the spectrograms. The stability of 0.3 Hz in spectrograms indicates that oceanic conditions were quite stable during the recording of present mCSEM data.

Figure 6 shows that the power of a microseism is significant even when the transmitter current is 'on'. Overall, the time series analysis suggests that features like microseism and swell induce a significant electric field at the seafloor to contaminate the mCSEM data. Proper measures for removal of the noise are essential for a better interpretation of mCSEM data.

**Acknowledgement**

We thank KMS Technologies –KJT Enterprises Inc. for sponsoring the work.

**References**

1. Bhatt, K. M., A. Hördt, P.Weidelt, T. Hanstein, 2009. Motionally induced electromagnetic field within the ocean, 23. Kolloquium Electromagnetische Tiefenforschung (EMTF), Brandenburg, Germany, September-October, this issue.
2. Chave, A.D., and C.S. Cox, 1982. Controlled electromagnetic sources for measuring electrical conductivity beneath the oceans, 1, forward problem and model study, J. Geophys. Res., 87, 5327-5338.
3. Chave, A.D., and D.S. Luther, 1990. Low-frequency, motionally induced electromagnetic fields in the ocean, 1, theory, J. Geophys. Res., 95, 7185-7200.
4. Chave, A.D., and J.H. Filloux, 1984. Electromagnetic induction fields in the deep ocean off California: oceanic and ionospheric sources, Geophys. J. R. astr. Soc., 77, 143-171.
5. Constable, Steven and Leonard J. Srnka, 2007. An introduction to marine controlled-source electromagnetic methods for hydrocarbon exploration, Geophysics, vol. 72, no. 2, p. wa3–wa12.
6. Crews, A., and J. Futterman, 1962. Geomagnetic micropulsation due to the motion of ocean waves, J. Geophys. Res., 67, 299-306.

7. Dahm T, F. Tilmann, J. P. Morgan, 2006. Seismic broadband ocean-bottom data and noise observed with free-fall stations: experiences from long-term deployments in the North Atlantic and the Tyrrhenian Sea, Bull. Seismol. Soc. Am, 96, 647–664, doi: 10.1785/0120040064.
8. Elgar, S. ,2008. Ripples run deep, Nature, Vol 455, Page 888.
9. Longuet-Higgins, M.S., E. Stern, H. Stommel, 1954. The electrical field induced by ocean currents and waves with application to the method of towed electrodes, Pap. Phys. Oceanog. Meteorol., 13(1),1-37.
10. Longuet-Higgins, M.S., 1950. A theory of the origin of microseisms, Philos.Trans. R. Soc. London, Ser. A, 243, 1–35.
11. Podney, W., 1975. Electromagnetic fields generated by ocean waves, J. Geophys. Res., 80, 2977-2990.
12. Sanford, T.B., 1971. Motionally induced electric and magnetic fields in the sea, J. Geophys. Res., 76, 3476-3492.
13. Tanimoto, T., 2005. The oceanic excitation hypothesis for the continuous oscillations of the Earth, Geophy. J. Int., 160, 276-288.
14. Webb, S.S. and C.S. Cox, 1985. Observation and modelling of seafloor microseisms, J. Geophys. Res., 91, B-7, 7343-7358.
15. Welch, P. D. 1967. The use of fast-Fourier transform for the estimation of power spectra: A short method based on time averaging over short, modified periodograms, IEEE Transactions of the Audio and Electroacoustics, AUlS, 70-13.